

Exploring Self-Supervised Learning for SAR ATR: A Knowledge-Guided Predictive Perspective

Weijie Li^a, Wei Yang^{a,*}, Tianpeng Liu^a, Yuenan Hou^b, Yuxuan Li^c, Zhen Liu^a, Yongxiang Liu^{a,*} and Li Liu^{a,*}

^athe College of Electronic Science and Technology, National University of Defense Technology, Changsha, 410073, China

^bthe Shanghai AI Laboratory, Shanghai, 200000, China

^cthe Visual Computing and Intelligent Perception Lab, Nankai University, Tianjin, 300071, China

ARTICLE INFO

Keywords:

Synthetic Aperture Radar (SAR)
Automatic Target Recognition (ATR)
Self-Supervised Learning (SSL)
Deep Learning
Masked Image Modeling (MIM)

ABSTRACT

The growing availability of Synthetic Aperture Radar (SAR) target datasets allows for the consolidation of different SAR Automatic Target Recognition (ATR) tasks using a foundational model powered by Self-Supervised Learning (SSL). SSL aims to derive supervision signals directly from the data, thereby minimizing the need for costly expert labeling and maximizing the use of the expanding sample pool in constructing a foundational model. This study investigates an effective SSL method for SAR ATR, which can pave the way for building the foundation model. The primary obstacles faced in SSL for SAR ATR are the scale problem of the remote sensing images and speckle noise in SAR images. To overcome these challenges, we present a novel approach called Knowledge-Guided Predictive Architecture (SAR-KPGA), which leverages local masked patches to predict the multi-scale SAR feature representations of unseen context. The key aspect of SAR-KPGA is integrating SAR domain features to ensure high-quality target features for SSL. Furthermore, we employ local masks and multi-scale features to accommodate the large image scale and target scale variations in remote sensing scenarios. By evaluating our framework on three target recognition datasets (vehicle, ship, and aircraft), we demonstrate its outperformance over other SSL methods and its effectiveness with increasing SAR data. This study showcases the potential of SSL for SAR target recognition across diverse targets, scenes, and sensors.

1. Introduction

Synthetic aperture radar (SAR) possesses the capability to capture images under diverse weather and lighting conditions, rendering it indispensable for acquiring Earth observation information (Sun et al., 2021; Moreira et al., 2013; Tsokas et al., 2022). Serving as a crucial component in SAR image interpretation, SAR Automatic Target Recognition (ATR) aims to localize and classify desired targets within SAR images automatically. Over the past few decades, extensive research has been conducted in this field, resulting in various civilian and military applications, including transportation management (Gagliardi et al., 2023), autonomous driving (Rizzi et al., 2021), concealment detection (Frolind et al., 2011), and military surveillance (Li et al., 2023b; Peng et al., 2022). In the last decade, deep learning has revitalized SAR ATR, leading to remarkable advancements (Kechagias-Stamatis and Aouf, 2021; Li et al., 2023a; Datcu et al., 2023). Despite significant progress, the high costs associated with data collection and annotation limit dataset diversity and method applications. SAR ATR studies are categorized into subfields such as vehicle (Li et al., 2023b), ship (Hou et al.,

2020), and aircraft recognition (Zhao et al., 2022). Hence, an intriguing and worthwhile question to explore is *whether a generic representation and model exist for various SAR target recognition tasks*.

The emerging self-supervised learning techniques present a potential solution to this question. Self-supervised learning (SSL) aims to extract meaningful signals directly from the data, thereby reducing the need for costly expert annotations and efficiently using the growing number of samples. Foundation models, which are trained on extensive datasets using SSL, have demonstrated their effectiveness in various computer vision (Golub et al., 2023; He et al., 2022), remote sensing (Sun et al., 2023), and clinical medical tasks (Zhou et al., 2023b). Consequently, we posit that foundation models, trained through SSL on a large dataset, can yield a generalized representation for SAR target recognition. To this end, this paper investigates the key challenges in SSL for SAR ATR.

Lack of a large-scale pre-training set. Just as ImageNet (Fei-Fei and Krishna, 2022) has achieved an impressive contribution to computer vision by pushing the number of categories for object recognition from twenty to thousands, a large-scale pre-training set for SAR target recognition will bring new research ideas and tasks. Unfortunately, due to the acquisition cost and annotation difficulties, many SAR target datasets have at most ten annotation categories and a few thousand images. Whereas some studies (Huang et al., 2022; Zhai et al., 2022; Pei et al., 2023) in SAR target

*This document was supported by the National Key Research and Development Program of China (No. 2021YFB3100800), the National Natural Science Foundation of China (No. 61871384, 61901487, 61901498, and 61921001), and the Science and Technology Innovation Program of Hunan Province (No. 2022RC1092).

*Corresponding author

✉ lwj2150508321@sina.com (W. Li); yw850716@sina.com (W. Yang);
everliutianpeng@sina.cn (T. Liu); houyuenan@pjlab.org.cn (Y. Hou);
yuxuan.li.17@ucl.ac.uk (Y. Li); zhen_liu@nudt.edu.cn (Z. Liu);
lyx_bible@sina.com (Y. Liu); dreamliu2010@gmail.com (L. Liu)

recognition used a few datasets as pre-training and evaluations, the potential of self-supervised learning in large-scale SAR datasets has yet to be explored fully. Therefore, it is necessary to integrate increasing open-source datasets to construct a large-scale pre-training set containing diverse targets, scenes, and sensors¹.

Special properties of SAR images. SAR achieves coherent imaging through a moving platform, which belongs to a remote sensing view. Its images capture the electromagnetic scattering of objects, but they are often affected by multiplicative speckle noise, phase errors, and other interferences. Consequently, SAR image interpretation is extremely difficult and poses difficulties for SSL methods. Our study focuses on addressing two key issues: the scale problem and target features. Firstly, remote sensing images often contain large scenes and small targets, making it difficult to learn effective contextual information for targets. However, current pre-training methods for SAR target recognition focus less on this issue because they have mainly focused on a few datasets that lack significant scale problems in the dataset. Secondly, SAR images are affected by speckle noise, which can impact the quality of learned representations. Current studies attempted to address this issue through data augmentation (Zhai et al., 2022) and filtering methods (Pei et al., 2023) in contrastive SSL, as well as Histogram of Oriented Gradients (HOG) features (Wang et al., 2023c) in generative SSL. However, data augmentation in contrastive learning can not simulate the effects of speckle noise exactly, and the gradient computation in HOG features is not well-suited to multiplicative noise. From the above discussions, these two issues still require adequate solutions. We aim to leverage SAR domain knowledge to address these unique challenges for SSL effectively.

In order to deploy self-supervised learning for SAR ATR, we first constructed a pre-training dataset consisting of approximately 100,000 SAR magnitude images sourced from publicly available datasets (Xia et al., 2022; Chen et al., 2022b; Wang et al., 2019; Malmgren-Hansen et al., 2017; Kusk et al., 2016; Lewis et al., 2019). This dataset encompasses a wide range of target classes, scenes, and sensors, allowing us to explore effective self-supervised learning methods. To address the abovementioned issues, we proposed a novel architecture called Knowledge-Guided Predictive Architecture for SAR ATR (SAR-KGPA²) in Figure 1. SAR-KGPA leverages domain-specific knowledge in SAR imaging and incorporates the Masked Image Modeling (MIM) task to learn contextual relationships within the SAR feature space. We employed the well-established gradient-by-ratio method (Dellinger et al., 2014; Song et al., 2016) for feature extraction, which effectively mitigates the impact of speckle noise in SAR images and facilitates accurate target shape extraction. Furthermore, we introduced local masks

¹ Various imaging conditions regarding target, scene, and sensor can lead to complex target and background signature variations in SAR images (Ross et al., 1999; Li et al., 2023b).

² Our codes: <https://github.com/waterdisappear/SAR-KGPA>

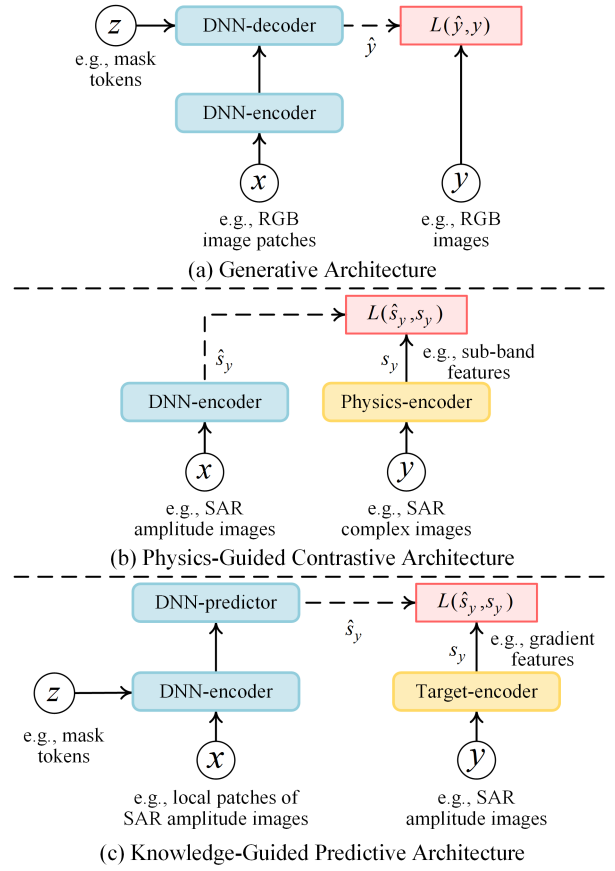


Figure 1: Our architecture for self-supervised learning with SAR target recognition. (a) Generative architectures (He et al., 2022) focus on reconstructing the pixels of unseen patches with a high mask proportion. This approach creates a challenging and meaningful pretext task that allows the model to learn contextual relationships within images. (b) Physics-guided contrastive architectures (PGCA) (Datcu et al., 2023; Huang et al., 2022) leverage the unique representation in the SAR domain as guided signals to constrain the representation of the Deep Neural Network (DNN). By incorporating physical principles into the learning process, PGCA enhances the model's ability to capture accurate and important SAR features. (c) Our knowledge-guided predictive architectures (SAR-KGPA) combine SAR domain knowledge and the meaningful MIM pretext task to learn contextual relationships in the SAR feature space. This approach utilizes prior knowledge about SAR target recognition in target scale and features to improve the representation.

and multi-scale features to enhance the architecture's adaptability to different image and target scales in the context of remote sensing vision. To evaluate the effectiveness of our proposed architecture, we conducted experiments on three datasets (vehicle (Air Force Research Laboratory), ship (Sun et al., 2022), and aircraft (Sun et al., 2022)).

The results demonstrate that SAR-KGPA achieves improved performance than other SSL methods. Importantly, it can increase with the volume of pre-training data, thereby showing the potential of self-supervised learning to build a foundation model to unify SAR ATR across different targets,

scenes, and sensors. In summary, the main contributions of this article are as follows:

- We proposed a knowledge-guided predictive architecture that incorporates SAR domain knowledge and mask image modeling. Our research highlights the importance of leveraging SAR domain knowledge, specifically addressing the scale problem and target features, to ensure the generalization of self-supervised learning.
- Our work conducted a comprehensive pre-training study with SSL for SAR target recognition. Performance with increasing data volume demonstrates the potential of SSL to learn generalized feature representations and will stimulate the research enthusiasm for the fundamental models on SAR target recognition.

The remainder of this paper is organized as follows. Sec. 2 introduces related studies in self-supervised learning and SAR target recognition. Sec. 3 introduces the proposed knowledge-guided predictive architecture. Sec. 4 conducts extensive experiments and analyses for the two special issues and scaling ability for SSL on SAR ATR. Sec. 5 concludes the whole paper and discusses the limitations.

2. Related Work

2.1. Self-supervised learning

Self-supervised learning (Liu et al., 2021; Balestrieri et al., 2023) aims to learn the intrinsic relationship in samples through a pretext task. This method can leverage a huge amount of unlabelled data and perform well in various downstream tasks. Self-supervised learning methods can be broadly categorized into contrastive and generative approaches (Liu et al., 2021). In this study, we focus on generative masked image modeling because it can model both local and long-range information (Xie et al., 2023b), and the data augmentation pretext task in the contrastive approach is not fully compatible with the SAR image properties. BEiT (Bao et al., 2021) proposed the concept of masked image modeling and predicted the masked patches in a frozen pre-training tokenized space. Compared to BEiT, MAE (He et al., 2022) achieved an efficient and meaningful task through asymmetric autoencoder structure and high masking rate. Furthermore, SimMIM (Xie et al., 2022) showed that masked image modeling can be achieved with a simple structure, such as a linear projection layer and a random mask. Over time, a series of improvement works have emerged, and our focus is on research in masking methods and target features.

Masking strategy can affect the representation quality, which is centered on ensuring pretext task difficulty and learning contextual information around target regions. MAE (He et al., 2022) and SimMIM (Xie et al., 2022) compared different sampling strategies, such as random sampling, block sampling, and grid sampling, and found that random sampling with a large mask ratio works best. I-JEPA (Assran et al., 2023) employed block sampling

and used a single context block to predict several non-overlapping target blocks to exploit the rich semantics in the context block. Hard patches mining (Wang et al., 2023a) applied a teacher network to predict the reconstruction loss of different patches to better mine the target foreground region. PixMIM (Liu et al., 2023) used a simple random resized crop to preserve more of the target foreground region in the random mask for semantic concept learning. Inspired by the fact that target reconstruction in MAE mainly uses the surrounding area, Local Masked Reconstruction (LoMaR) (Chen et al., 2022a) proposed to perform masked reconstruction within a local image block instead of the whole image to improve computational efficiency. As for remote sensing images, the masking strategy must consider their large scene and small target properties. We applied the LoMaR method to learn local contextual information.

Target features. Masked image modeling learns contextual information by reconstructing and predicting various feature representations, such as pixel values (He et al., 2022; Xie et al., 2022), discrete tokens (Bao et al., 2021), HOG features (Wei et al., 2022; Wang et al., 2023b), deep features (Wei et al., 2022; Assran et al., 2023), and frequency features (Xie et al., 2023a; Liu et al., 2023). MaskFeat (Wei et al., 2022) proved that the target features can be either the classical HOG feature or deep features obtained by other self-supervised methods. LocalMIM (Wang et al., 2023b) performed multiscale reconstruction of HOG features at different encoder layers to facilitate representation learning speed and semantic understanding of scales. I-JEPA (Assran et al., 2023) used a learnable target encoder to get deep semantic features. PixMIM (Liu et al., 2023) enhanced the learning of low-frequency components such as target shape by reconstructing the image after low-pass filtering. Masked frequency modeling (Xie et al., 2023a) avoided spatially redundant masking by reconstructing different frequency components. A priori knowledge can be incorporated as a target feature to guide representation learning. Therefore, we used the gradient-by-ratio method in SAR to extract the target edge shape features and suppress the speckle noise.

2.2. Self-supervised learning in remote sensing

In recent years, there has been a growing interest in self-supervised learning for remote sensing, which provides a paradigm for solving the contradiction between increasing samples and the lack of high-quality annotations (Wang et al., 2022b). Self-supervised learning has many applications in multi-source data such as multispectral (Reed et al., 2023; Sun et al., 2023), hyperspectral (Ibanez et al., 2022), and SAR (Wang et al., 2023c; Huang et al., 2022; Zhai et al., 2022) with various paradigms of contrastive and generative.

Due to the lack of a large-scale dataset, self-supervised learning in SAR ATR is relatively scarce (Zhai et al., 2022; Pei et al., 2023; Li et al., 2023b; Wen et al., 2021). These studies rely on contrastive learning or target rotation angle information. However, data augmentation methods applied on natural images may not be fully suitable for SAR images (Wang et al., 2022b). For example, Gaussian blurring

and noise methods can not simulate multiplicative speckle noise effects, and the rotation is incompatible with SAR images because of the anisotropic electromagnetic scattering. In addition, only a few datasets provide information on the target rotation angle. Compared to applying multiple data augmentation methods to simulate the imaging condition variations and noise interference for SAR images (Zhai et al., 2022; Pei et al., 2023; Li et al., 2023b), we prefer another contrastive architecture (Datu et al., 2023) compatible with SAR images' properties. Its contrastive architecture used a priori knowledge to extract features to guide representation learning. We combine this idea with MIM to learn contextual semantic information within the feature space. And the target features with the SAR image properties can ensure a high-quality representation. We discuss self-supervised learning in remote sensing and SAR from three aspects.

Pre-train dataset. There is no unified benchmark setting for self-supervised learning with SAR target recognition due to the lack of a large dataset such as ImageNet. For scene classification (Wang et al., 2023c; Huang et al., 2022), the pre-training sets used BigEarthNet-MM (Sumbul et al., 2021) or the sea ice dataset (Huang et al., 2022). For target recognition (Zhai et al., 2022; Pei et al., 2023), the pre-training sets applied the MSTAR vehicle (Air Force Research Laboratory) or OpenSAR ship (Huang et al., 2017) datasets. Previous work for SAR target recognition (Zhai et al., 2022; Pei et al., 2023) used pre-training sets that contain several target categories and scenarios. Therefore, the potential of self-supervised learning for foundation models in SAR target recognition has yet to be investigated. Constructing a more large dataset containing various targets, scenes, and sensors is necessary.

Scale of target and scene. A major difference between remote sensing and computer vision is in scene range and target size. Remote sensing images usually contain large scenes and small targets (Li et al., 2023c; Cheng et al., 2023). TOV (Tao et al., 2023) illustrated that small scenes with different semantics within a larger scene affect contrastive learning. Chen et al. (Chen and Bruzzone, 2022) used shift alignment of two local regions between SAR and optical images in contrast learning. RingMo (Sun et al., 2023) proposed a PIMask sampling strategy for dense small targets in remote sensing images, *i.e.*, secondary pixel sampling of the masked patches to expose small targets. However, we found that pixel sampling does not work for SAR images because the single pixels of SAR images contain multiplicative noise. Therefore, we prefer local patches for masking instead of the whole image or pixel level.

SAR speckle noise. Speckle noise affects the quality of self-supervised learning features, so the researcher has used many ways, such as data augmentation (Zhai et al., 2022), filtering (Pei et al., 2023), and feature extraction, to address the problem. Zhai et al. (Zhai et al., 2022) added Gaussian noise and blur to data augmentation methods. But Gaussian noise and blurring do not perfectly match multiplicative speckle noise. Pei et al. (Pei et al., 2023) used the despeckling pre-processing method in contrastive

learning to address speckle noise. We focus on how to extract high-quality features as guidance signals. Similarly to our work, Wang et al. (Wang et al., 2023c) discussed different features such as CannyEdge (Canny, 1986), HOG, and SAR-SIFT (Dellinger et al., 2014) features for SAR scene classification and segmentation. They found HOG is more appropriate than SAR-SIFT for SAR images. Our work aims to mine semantic information at the target level rather than the scene level through local patches. For multiplicative speckle noise, we find that gradient-by-ratio is more suitable for target shape information extraction than HOG's differential gradient in self-supervised learning for SAR ATR. Our proposed framework accomplishes noise reduction and feature extraction to ensure high-quality representation.

3. Approach

The proposed Knowledge-Guided Predictive Architecture for SAR ATR (SAR-KGPA) is illustrated in Figure 2. Our overall objective is as follows: given local masked patches, predict feature representations in the SAR domain. Therefore, the model can achieve SAR image interpretation by recognizing the contextual relationship between the target parts and the surrounding area.

As shown in Figure 2, the input is the single-channel SAR magnitude image since most target datasets are magnitude pictures. We randomly select different local patches and add mask tokens according to LoMaR (Chen et al., 2022a). Vision Transformers (ViT) (Dosovitskiy et al., 2020) in MAE are used as the DNN-encoder and DNN-predictor. Each local masked patch is fed into the MIM structure to predict the target feature of mask tokens.

Importantly, the special SAR coherent imaging mechanism requires domain knowledge to predict target features. SAR coherent imaging results in multiplicative scattering noise in the magnitude image, and we use the gradient-by-ratio (Dellinger et al., 2014; Song et al., 2016) to suppress the speckle noise and extract the targets' edge and shape. Moreover, we employ a multi-scale setting for various targets in the pre-training set.

3.1. Local Masked Patches

We aim to learn the contextual relationship of various targets. Whereas such relationships normally remain in small areas due to the large scale and small target in remote sensing imagery. Therefore, we perform masking in the local patches following LoMaR. Although LoMaR is designed to improve computational efficiency, we find this local setting is suited for small targets in remote sensing. According to the LoMaR, mask tokens and relative positional encoding (Wu et al., 2021) are added to the encoder input and MAE structure to enhance the feature representation.

3.2. Target Encoder

Due to the SAR imaging mechanism (Moreira et al., 2013), the images' amplitude values contain multiplicative speckle noise. The speckle noise is related to the sensor resolution and is caused by the coherent superposition of

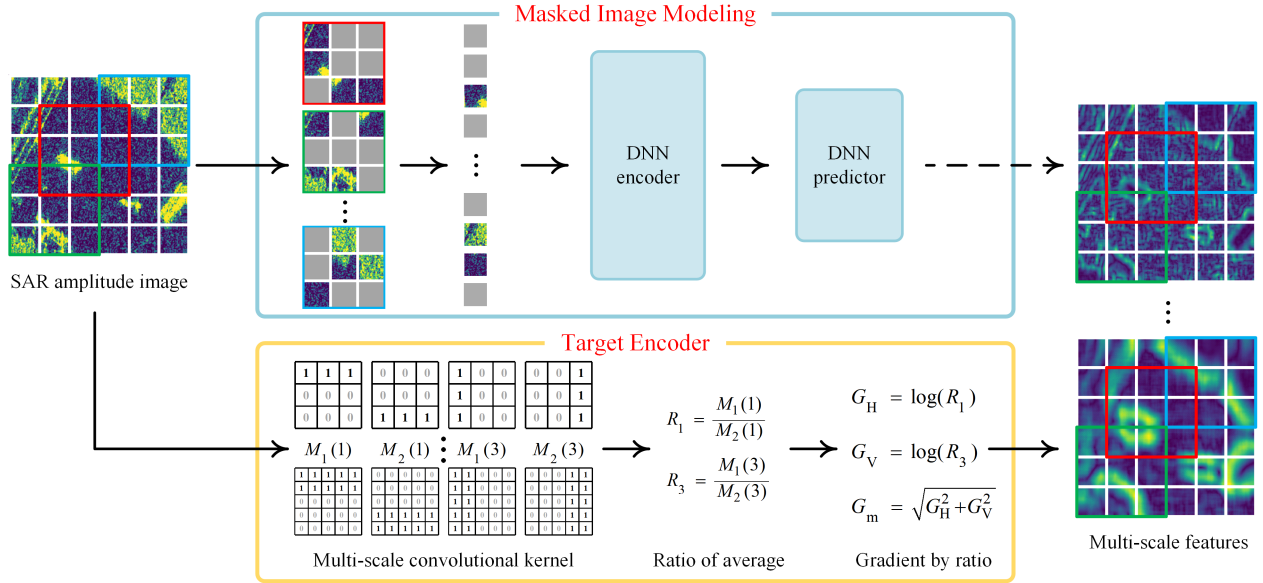


Figure 2: The overall framework of SAR-KGPA. The proposed Knowledge-Guided Predictive Architecture for SAR target recognition (SAR-KGPA) uses locally masked patches to predict the multi-scale SAR feature representations of unseen patches. The MIM structure uses the Vision Transformer (ViT) in MAE. The DNN encoder extracts deep features of masked patches, and the DNN predictor predicts SAR features of unseen patches. The target encoder uses the gradient-by-ratio method to map SAR images from pixel space to feature space, thus extracting the target shapes and avoiding speckle noise interference in SAR images. Local patches and multi-scale features are designed for multi-scale small targets in remote sensing.

different scatterers within the scattering cell. Therefore, reconstructing image pixels for SAR images receives noise interference and fails to learn a high-quality feature representation. This problem of speckle noise can be solved by filtering and feature extraction. However, filtering has a conflict between noise reduction and image details, and we use feature extraction. Some studies have proposed different types of target features in computer vision, mainly divided into traditional manual features (Wei et al., 2022) and deep learning features (Assran et al., 2023). However, these methods are difficult to migrate to SAR target recognition directly, so we combine the traditional local description feature extraction methods (Dellinger et al., 2014; Song et al., 2016; Dong et al., 2020) in the SAR domain.

Gradient computation. The classical differential gradient is not a constant false alarm rate operator due to multiplicative speckle noise in the SAR image, and previous studies (Touzi et al., 1988; Bovik, 1988) have shown that the computing ratio is more suitable for multiplicative noise. Here, we use the simplest ratio of average (ROA) (Touzi et al., 1988) not to blur image details:

$$R_i = \frac{M_1(i)}{M_2(i)}, \quad (1)$$

where R_i denotes the average ratio at different directions and $M_1(i)$ and $M_2(i)$ are the area averages on opposite sides of the current pixel along direction i . $i = 1$ is the horizontal direction and $i = 3$ means the vertical direction. As shown in Figure 2, the area averages can be computed from the input image and four fixed convolution kernels.

The use of logarithms can solve the vertical gradient calculation (Dellinger et al., 2014), and the horizontal and vertical gradients are defined as:

$$\begin{aligned} G_H &= \log(R_1) \\ G_V &= \log(R_3) \end{aligned} \quad (2)$$

where G_H is the horizontal gradient and G_V is the vertical gradient. The gradient magnitude is $G_m = \sqrt{G_H^2 + G_V^2}$.

Multi-Scale Feature. SAR-HOG (Song et al., 2016) has discussed the kernel sizes for SAR vehicle target recognition and given the best single size for the MSTAR vehicle dataset. However, a single-size kernel cannot accommodate various targets when the dataset is extended to different targets and scenes. Due to the dynamic range of contextual information for various targets in remote sensing (Li et al., 2023c), a multi-scale feature is constructed with convolutional kernels of different sizes in Figure 1. We set the kernel scale r equal to 5, 7, 13, and 17, and the whole convolutional kernel size is odd square $2r + 1$. As shown in Figure 1, small-scale convolutional kernels provide a finer extraction of small target contours, while large-scale convolutional kernels focus on large targets and scene edges and noise suppression.

3.3. Implementation

Given SAR images, we randomly sample several square windows at different spatial locations as local patches and mask each patch with mask tokens at a fixed percentage. Then, each local masked patch's visible and unseen parts are fed into the MIM structure, whose encoder and predictor are applied with learnable relative positional encoding in

Table 1

Description of SAR datasets used for pre-training. # Target: Number of target categories. # Scene: Number of scenes. Res.: Resolution. Large SAR imagery in the detection contains more target and scene types than the annotation.

Dataset	Size	# Target	# Scene	Res. (m)	Band	Polarization	Description
MSAR	28,499	≥ 4	≥ 6	1	C	Quad	Ground and sea targets detection dataset
SAR-Ship	39,729	≥ 1	≥ 4	3~25	C	Quad	Ship detection dataset in complex scenes
SARSim	21,168	7	3	0.3	X	Single	Vehicle simulation dataset
SAMPLE	5,380	10	1	0.3	X	Single	Vehicle simulation and measured dataset

the self-attention layer. Meanwhile, the whole SAR image is provided to the target encoder. The average values in four directions are obtained after multi-scale convolution in four directions. Then, the gradients by ratio are obtained as multi-scale SAR features by the ratio and logarithm operations. The loss function computes the mean squared error in the feature space between the DNN features and SAR multi-scale features for masked patches. In addition to the major improvement of the target encoder, there are two other minor.

Data augmentation. We follow the simple data augmentations in MAE and add a random contrast adjustment for SAR magnitude images.

Decoder design. While some work (Chen et al., 2022a; Wei et al., 2022) has shown that it is feasible to use a simple linear head as a decoder or predictor for self-supervised learning in RGB images, we find that a ViT with eight layers in the MAE is less disturbed by SAR image noise than a linear layer, allowing the encoder to extract deep semantic features of targets.

4. Experiments

This section analyzed the proposed architecture. We first described the pre-training and few-shot classification experimental setting in Sec. 4.1. Then, the proposed SAR-KGPA was compared with other methods in Sec. 4.2. We then discussed the local mask region in Sec. 4.3 and performed an ablation study for the SAR-KGPA with different target features in Sec. 4.4. In the end, Sec. 4.5 discussed the scaling experiment of our methods and showed improved performance with increasing data volume.

4.1. Dataset and Experimental Settings

We examine self-supervised learning performance with the following procedure. First, we perform the self-supervised learning on the pre-training dataset without label information. Then, we fine-tune the pretrained model on few-shot SAR classification datasets.

Pre-training. Pre-training datasets are designed to ensure rich information about targets, scenes, and sensors. Therefore, we chose four datasets covering popular targets (vehicles, ships, aircraft, etc), complex backgrounds (ground and ocean), and various sensors (satellite-borne, airplane-borne, and simulation) in Table 1 and Figure 3.

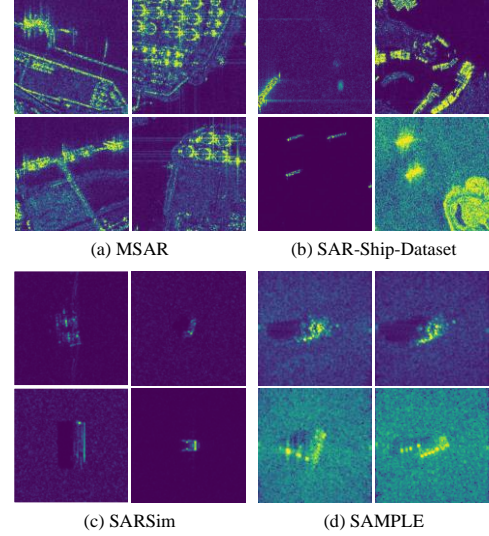


Figure 3: Datasets for the pre-training contain different targets, scenes, and sensors. MSAR is the satellite-based dataset of ground and sea targets; SAR-Ship-Dataset is the satellite-based dataset of sea targets; SARSim is the multi-angle simulation dataset of vehicle targets; and SAMPLE is the simulated and measured dataset of vehicle targets.

- **MSAR** (Xia et al., 2022; Chen et al., 2022b) is a multi-class target detection dataset based on the Chinese HISEA-1 satellite in large-scale scenes. MSAR comprises 28,449 image slices with quad polarization. Scenes covered include airports, harbors, nearshore, islands, distant seas, urban areas, etc. The labeled target categories include aircraft, oil tanks, bridges, and ships. This dataset can provide target samples in complex ground and sea scenes.
- **SAR-Ship** (Wang et al., 2019) dataset is a ship detection dataset in complex scenes based on Chinese Gaofen-3 and European Sentinel-1 satellites. The public version of this dataset contains 39,729 images from two satellites in different imaging modes and resolutions. The dataset provides ship targets of various sizes in complex ocean scenes such as nearshore, distant seas, harbors, and islands.
- **SARSim** (Malmgren-Hansen et al., 2017; Kusk et al., 2016) is a fine-grained vehicle dataset created by Terma A/S, Denmark. The simulation system used for this dataset can generate X-band SAR images

with resolutions ranging from 0.1m to 0.3m from CAD models. Sarsim provides 21,168 vehicle samples in 7 categories (truck, car, motorbike, bus, tank, bulldozer, and pickup) and 3 scenes (grass, roads, and a mean of the two) with 7 imaging depression angles. This dataset provides fine-grained differences between targets.

- **SAMPLE** (Lewis et al., 2019) is a fine-grained synthetic and measured paired vehicle dataset released by the Air Force Research Laboratory, USA. This dataset is simulated in X-band and 0.3m resolution. The public version of this dataset provides 5,380 images of ten categories of military vehicle targets at partial imaging angles, and five categories overlap with the public version of MSTAR. As shown in Figure 3, it can be noticed that the ground clutter in SAMPLE is more significant and realistic than in Sarsim.

Downstream tasks. We tested the pre-trained model on three target recognition datasets to evaluate the ability for fine-grained semantic classification in the case of small samples with fine-tuning and linear probing. According to MAE, fine-tuning is tuning all model parameters, and linear probing is tuning a linear layer with batch normalization while freezing other parameters.

- **MSTAR** (Air Force Research Laboratory) is the most commonly used SAR target classification dataset released by the Defense Advanced Research Projects Agency, USA, which contains ten categories of vehicles with different angles, variants, and other imaging conditions. It has many experimental setting variants, while we refer to the (Li et al., 2023b) to adopt the most commonly used ten-class classification settings to evaluate the fine-grained classification performance for SAR vehicles.
- **FUSAR-Ship** (Sun et al., 2022) contains 15 primary ship categories and many non-ship targets based on the Gaofen-3 satellite in scenes such as sea, land, coast, river, and island. Based on the experimental setting of (Wang et al., 2022a), we have ten types of ocean target slices from origin images, such as four fine-grained ships, bridges, and ocean scene slices. We use this dataset to evaluate the fine-grained classification performance for ocene targets.
- **SAR-ACD** (Sun et al., 2022) contains six types of aircraft based on the Gaofen-3 satellite in three civil airports, including Shanghai Hongqiao Airport, Beijing Capital Airport, and Taiwan Taoyuan Airport. Since the released dataset does not separate the training and test data, we randomly select small samples as the training set and others as the test set. We use this dataset to evaluate fine-grained aircraft target classification. Fine-grained recognition of aircraft targets is a more challenging task due to the smooth surface of the aircraft, resulting in insignificant features.

Experimental settings. Table 2 gives the default setting. The pre-training is applied on 4 NVIDIA V100 GPUs with

Table 2
Experimental setting.

Pre-training setting	
Config	Value
optimizer	AdamW
base learning rate	1e-3
weight decay	0.05
optimizer momentum	$\beta_1, \beta_2 = 0.9, 0.95$
batch size	300
epoch	200
learning rate schedule	cosine decay
warmup epoch	20
augmentation	ResizedCrop, HFlip, Contrast
Classification settings	
Config	Value
optimizer	AdamW
base learning rate	1e-3
weight decay	5e-4
optimizer momentum	$\beta_1, \beta_2 = 0.9, 0.999$
batch size	50
epoch	40
learning rate schedule	cosine decay
warmup epoch	2
warmup type	constant
warmup learning rate	1e-5

200 epochs and 300 batch sizes, and the backbone model is ViT-Base. Other hyperparameters of each method use the default settings from their papers and codes. Compared to the training settings of MAE, we add ColorJitter (contrast = 0.5) to increase data richness. All models use the same training settings in downstream classification tasks. The few-shot learning setting is based on the Dsssl toolbox (Zhou et al., 2023a) and is averaged over 10 random experiments.

4.2. Comparisons with other methods

As shown in Table 3, we evaluated the SSL methods in few-shot classification tasks. The comparison methods are ImageNet, MAE (He et al., 2022), Feature Guided MAE (FG-MAE) (Wang et al., 2023c), I-JEPA (Assran et al., 2023), LoMaR (Chen et al., 2022a), PGCA (Datcu et al., 2023), and Our SAR-KGPA. Table 3 also gives the difference in the mask area and target features. The ImageNet migrated the supervised pre-training weights on the ImageNet as initialization. Following the PGCA using complex SAR image's features as target signal, we used our SAR gradient features for pixel-level contrastive learning to test the effectiveness of SAR feature, *i.e.*, mask image modeling is removed from SAR-KGPA.

Table 3 studies the result of different pre-trained models on fine-grained SAR target classification. Due to the large difference between SAR and RGB images, ImageNet weights are hard to obtain effect features with small samples with fine-tuning, and using linear probing can have a better result with an unsuitable initialization weight. MAE trained on the SAR dataset performs better than ImageNet with fine-tuning, but the speckle noise affects its representation

Table 3

Fine-grained classification results of different methods. The classification metric is average accuracy (%). **Bold** indicates the best result, underline indicates the next best result.

MSTAR								
Method	Mask area	Target feature	fine-tuning			linear probing		
			10-shot	20-shot	40-shot	10-shot	20-shot	40-shot
ImageNet	-	-	16.7	32.0	40.7	45.0	56.3	66.8
MAE (He et al., 2022)	Global	Pixel value	50.6	61.3	69.5	53.7	59.2	63.7
FG-MAE (Wang et al., 2023c)	Global	HOG	50.0	58.7	70.0	43.5	50.7	56.4
I-JEPA (Assran et al., 2023)	Global	Deep feature	24.5	33.4	44.6	30.9	38.6	44.7
LoMaR (Chen et al., 2022a)	Local	Pixel value	45.6	62.9	77.0	39.3	48.9	55.6
PGCA (Datcu et al., 2023)	Local (No mask)	GR (ours)	<u>56.7</u>	<u>71.4</u>	<u>88.1</u>	<u>61.0</u>	<u>68.0</u>	<u>74.7</u>
SAR-KGPA	Local	GR (ours)	70.3	82.1	91.6	67.7	75.1	81.6

FUSAR-ship								
Method	Mask area	Target feature	fine-tuning			linear probing		
			10-shot	20-shot	40-shot	10-shot	20-shot	40-shot
ImageNet	-	-	54.0	57.0	59.7	74.6	79.6	83.6
MAE (He et al., 2022)	Global	Pixel value	71.7	75.4	78.2	74.2	78.1	80.3
FG-MAE (Wang et al., 2023c)	Global	HOG	65.5	73.7	76.6	69.7	74.3	77.7
I-JEPA (Assran et al., 2023)	Global	Deep feature	38.5	38.9	49.4	36.5	42.2	46.8
LoMaR (Chen et al., 2022a)	Local	Pixel value	75.9	80.2	82.7	70.5	77.9	80.7
PGCA (Datcu et al., 2023)	Local (No mask)	GR (ours)	<u>76.4</u>	<u>80.4</u>	<u>83.8</u>	<u>77.4</u>	<u>81.6</u>	<u>84.2</u>
SAR-KGPA	Local	GR (ours)	81.3	83.3	85.8	80.6	82.7	85.2

SAR-ACD								
Method	Mask area	Target feature	fine-tuning			linear probing		
			10-shot	20-shot	40-shot	10-shot	20-shot	40-shot
ImageNet	-	-	22.6	26.8	42.7	34.8	44.2	54.2
MAE (He et al., 2022)	Global	Pixel value	51.6	57.0	69.5	49.9	56.9	62.7
FG-MAE (Wang et al., 2023c)	Global	HOG	50.4	54.2	62.9	47.5	51.5	57.0
I-JEPA (Assran et al., 2023)	Global	Deep feature	45.0	51.7	63.3	42.7	51.0	60.0
LoMaR (Chen et al., 2022a)	Local	Pixel value	51.2	54.4	67.4	47.8	53.4	59.1
PGCA (Datcu et al., 2023)	Local (No mask)	GR (ours)	<u>51.8</u>	<u>60.0</u>	<u>73.7</u>	<u>52.7</u>	<u>58.3</u>	<u>66.1</u>
SAR-KGPA	Local	GR (ours)	54.8	62.6	75.5	56.8	60.4	66.8

quality. HOG is not an effective solution to the speckle noise because multiplicative noise leads to the virtual dots in the strong scattering region. It results in a performance degradation in FG-MAE with HOG features. Similarly, I-JEPA has the feature collapse, in which the learnable predictor fails to learn a good feature space under speckle noise. Therefore, we use gradient features with SAR domain knowledge as targets, and PGCA and SAR-KGPA have achieved a more significant performance than other methods. By combining mask image modeling and SAR domain knowledge, SAR-KGPA learns high-quality contextual features for low-quality noisy SAR data compared to PGCA.

Another interesting phenomenon is the range of contexts, where it can be found that LoMaR with local reconstruction can achieve better fine-tuning results in vehicle and ship compared to MAE. This result illustrates the need to consider the range of contextual information in remote-sensing images. However, due to a linear decoder, LoMaR is more susceptible to the effects of speckle noise in the pixels, leading to poorer linear probing results.

Although the proposed method achieves better results on the aircraft dataset, it is not as good as vehicle and ship results. It is because the aircraft reflects electromagnetic waves with its streamlined structure, resulting in SAR images that may lack the complete aircraft structure, with only some strong scattering points and shadow edges. Because of this, the generic representation in SAR images still needs to be further explored.

4.3. Visualization

Compared to supervised pre-training and contrastive learning, which have a local attention range in the high layer, ViT with MIM has various attention ranges in different layers (Xie et al., 2023b). However, Figure 4 shows that this characteristic of MIM is related to data property and pixel-level pretext task. We first notice that the deep layers of MAE mainly focus on global information due to large SAR image scenes, which differs from MIM's modeling properties with ImageNet. Then, LoMaR with local reconstruction acquires the ability to model local information. This phenomenon illustrates that local information is easily lost in remote

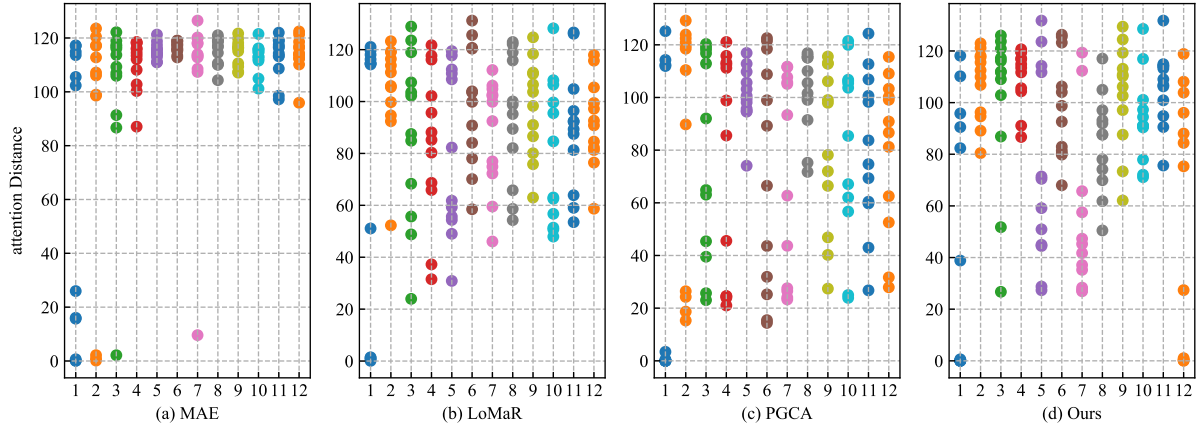


Figure 4: The averaged attention distance of ViT with different methods. The X-axis is the attention head *i.e.* layer number. MAE focuses on global information, and other methods have local and global attention ranges. It shows that using pixel-level features as a pretext task with a local image scale can enhance the diversity of ViT modeling with SAR images.

sensing images, and local reconstruction can better capture contextual details. In addition, PGCA, which removes the mask in SAR-KGPA and has a pixel-level contrast learning task, can acquire local information. It suggests that the property of modeling local and global information originates from the pixel-level pretext task. Finally, our SAR-KGPA with integrated MIM and PGCA can model local and global features. It can be found that the addition of MIM makes SAR-KGPA pay more attention to high-level global contextual information and more diminished attention to local edge features compared to PGCA. From the above discussions, the large remote sensing image challenges for MIM to learn effective representation, which is why we chose the LoMaR method to solve this problem.

4.4. Ablation Study

As for MIM based on SAR images, another key lies in extracting high-quality target features from low-quality and noisy SAR images. It needs to be combined with the SAR's physical knowledge. Here, we analyze the target feature selection and the multi-scale setting.

Target feature selection. In Table 4, we compare the results of pixel value, Low Pass Filter (LPF) (Liu et al., 2023), SAR-HOG (Song et al., 2016), and Gradient-by-Ratio (GR) (Dellinger et al., 2014). All the changes are made only in the target features, while other settings remain unchanged.

The Pixel in Table 4 uses MAE's ViT decoder, which suffers less noise interference than the LoMaR's single projection head. The LPF can mitigate noise interference, but we observe a slight drop of LPF compared to Pixel on the MSTAR's linear probing result. Therefore, inspired by the HOG feature in MaskFeat, we prefer to obtain high-quality target features further based on the suppressing noise.

Although HOG features have shown effectiveness in FG-MAE for SAR scene-level SSL, we found that the HOG features are unsuitable for target-level SSL in Table 4. This result is because speckle noise can make the gradient computation in small target regions appear to be many noise points,

greatly affecting the quality of target features. Inspired by the physics-guided contrastive architecture using SAR physics features, we investigate the HOG feature variant in the SAR domain, *i.e.*, SAR-HOG. The core of SAR-HOG is the change in the gradient calculation from differential gradient to ratio gradient. As shown in Table 4, we observe a significant improvement compared to HOG due to this modification. However, the sampling method of HOG may lead to the loss of some small target scattering points, such as the discrete points of an aircraft or a small boat. Therefore, we focus on the gradient information, *i.e.*, target edges. Moreover, basic information, such as the shape and edges of an object, is a generic property (Liu et al., 2022; Cheng et al., 2022; Shi et al., 2020).

We consider two versions of GR in SAR. One is computing gradient with a linear kernel (Song et al., 2016) whose value equals 1. Another is computing gradient with a Gaussian kernel (Dellinger et al., 2014) whose value obeys a Gaussian distribution. The Gaussian kernel can act as a filter, but the parameters need to be adjusted so as not to blur the target edges overly. For simplicity, we use a linear kernel without spending too much time tuning the parameters of the Gaussian kernel at different scales. Another important thing is that we propose a multi-scale setting instead of single-scale features due to the increased richness of targets included in the pre-training set.

Multi-scale setting. Multi-scale can improve the feature representation for various targets in remote sensing. Figure 5 gives the result of different kernel settings. Scale settings have various effects: smaller scales can better extract small target edges, while larger scales are more obvious for noise suppression. Hence, learning target features at different scales is more advantageous than a single scale.

4.5. Scaling Experiment

MIM can benefit from scaling data, model parameters, and computational resources, but it will suffer from overfitting when using small data and long training epochs on

Table 4

Results of different target feature for SAR-KGPA. The baseline is pixel value. LPF: low pass filter. HOG: histogram of oriented gradient. GR: gradient-by-ratio. The classification metric is average accuracy (%). **Bold** indicates the best result, underline indicates the next best result.

fine-tuning									
Method	MSTAR			FUSAR-Ship			SAR-ACD		
	10-shot	20-shot	40-shot	10-shot	20-shot	40-shot	10-shot	20-shot	40-shot
Pixel	55.3	69.8	84.5	78.6	82.0	84.8	51.7	60.1	71.7
LPF (Liu et al., 2023)	57.7	72.7	86.5	78.4	81.9	84.9	51.9	61.2	72.8
HOG (Wei et al., 2022)	30.2	32.4	40.3	58.1	63.3	66.6	51.7	57.9	64.7
SAR-HOG (Song et al., 2016)	<u>64.4</u>	76.4	<u>90.5</u>	76.7	80.8	85.3	51.4	60.0	73.4
GR (Dellinger et al., 2014)	62.8	<u>78.5</u>	88.2	80.6	82.8	86.0	55.3	62.9	73.0
GR (ours)	70.3	82.1	91.6	81.3	83.3	<u>85.8</u>	<u>54.8</u>	<u>62.6</u>	75.5

linear probing									
Method	MSTAR			FUSAR-Ship			SAR-ACD		
	10-shot	20-shot	40-shot	10-shot	20-shot	40-shot	10-shot	20-shot	40-shot
Pixel	57.7	64.4	72.2	78.0	81.0	84.0	54.4	58.9	64.4
LPF (Liu et al., 2023)	56.1	62.6	68.1	78.7	82.0	84.6	54.9	59.5	65.2
HOG (Wei et al., 2022)	33.3	37.8	41.6	52.6	58.3	61.5	49.2	53.1	56.7
SAR-HOG (Song et al., 2016)	58.9	68.1	77.1	79.3	81.8	85.0	54.6	59.3	66.5
GR (Dellinger et al., 2014)	<u>62.8</u>	<u>72.3</u>	<u>77.6</u>	82.0	82.9	85.7	<u>54.7</u>	60.9	<u>66.6</u>
GR (ours)	67.7	75.1	81.6	<u>80.6</u>	<u>82.7</u>	<u>85.2</u>	56.8	<u>60.4</u>	66.8

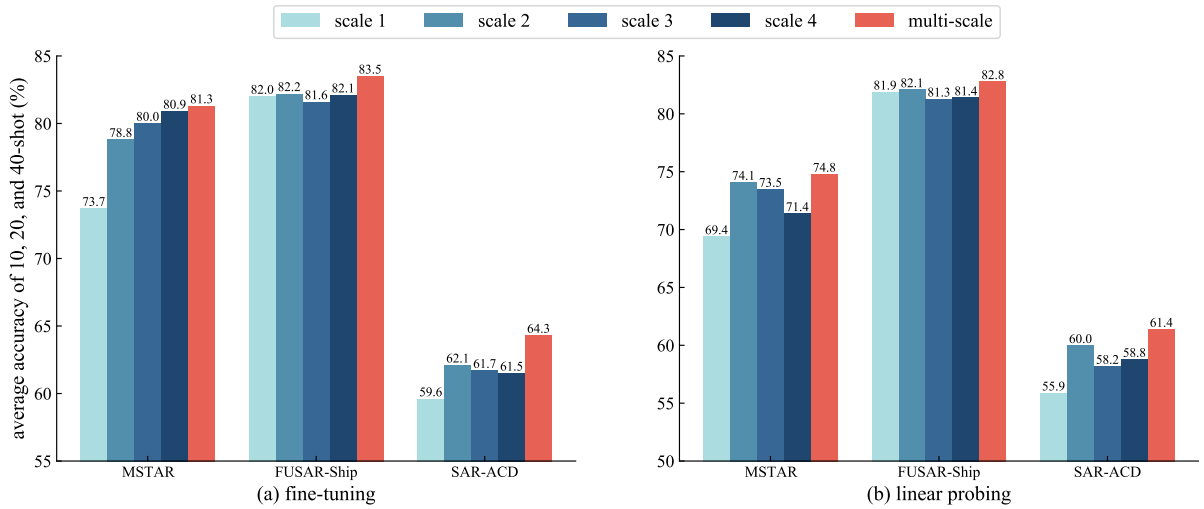


Figure 5: Multi-scale kernel settings for our gradient-by-ratio. Here, the scale 1/2/3/4 is with r equal to 5/7/13/17, and the multi-scale contains all four scales. Multi-scale is more suitable than single scale due to various targets in remote sensing images.

large models (Xie et al., 2023c). Therefore, we evaluate the scalability of SAR-KGPA with linear probing performance on SAR data. Figure 6 gives the scaling experiment in dataset size, model parameters, and training epoch.

Dataset size. A significant performance increase is observed in small-sample classification with increasing data volume. This phenomenon suggests that by extracting high-quality features as guide signals, self-supervised learning performance can be improved by increasing the number of noisy SAR images. Moreover, this result indicates that SSL does not reach saturation in dataset size and has a huge potential for foundation model to be exploited.

Model parameters. As the model parameters increase, we also observe an increase in representation quality. However, ViT-Large suffered from overfitting problems due to insufficient dataset size and has reduced performance in the fine-grained classification of vehicles and aircraft.

Training epoch. Similarly, too-long training epochs resulted in the overfitting of ViT-Base, and our default training setting is 200 epochs. Therefore, the next step is to collect more SAR target data to exploit the potential of SSL and foundation models.

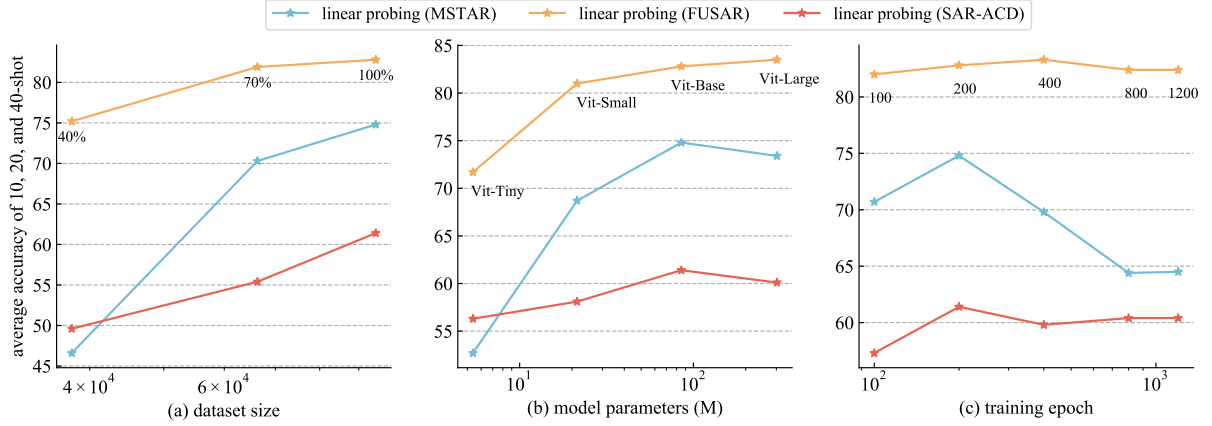


Figure 6: Scaling experiment of SAR-KGPA in dataset size, model parameters, and training epoch. We find that SAR-KGPA can benefit from these three aspects, but due to the limitation of dataset size, a large model and long training epochs lead to overfitting and reduce the linear probing performance.

5. Conclusion

In our work, we investigate the scale problem and target feature in MIM with SAR target images. By leveraging domain knowledge specific to SAR, we extend the applicability of MIM to SAR imagery, which is a type of noisy remote sensing data. Through extensive experimentation and analysis, we demonstrate the effectiveness of the proposed SAR-KGPA in obtaining high-quality feature representations for SAR ATR. Our research highlights the importance of embracing SSL to take advantage of the increasing availability of SAR data. The large pre-training samples give SSL the potential to achieve a foundation model for various downstream tasks across targets, scenes, and sensors.

However, it is worth noting that our pre-training dataset is not as extensive as ImageNet to fully exploit the potential of SSL for SAR ATR. In addition, it needs further investigation for other foundation model architectures, such as ConvNeXt. While our work primarily focuses on feature representation across different targets, it is essential to explore and discuss various tasks, including detection and segmentation. In the future, we plan to enhance our proposed scheme by improving data collection methods, refining model architectures, and exploring novel pre-training target features. Our ultimate goal is to successfully apply the foundation model with SSL in SAR target recognition.

References

- Air Force Research Laboratory. . The air force moving and stationary target recognition database. <https://www.sdms.afrl.af.mil/index.php?collection=mstar>.
- Assran, M., Duval, Q., Misra, I., Bojanowski, P., Vincent, P., Rabat, M., LeCun, Y., Ballas, N., 2023. Self-supervised learning from images with a joint-embedding predictive architecture, in: Proc. IEEE Comput. Soc. Conf. Comput. Vis. Pattern Recognit. (CVPR), pp. 15619–15629.
- Balestrieri, R., Ibrahim, M., Sobal, V., Morcos, A., Shekhar, S., Goldstein, T., Bordes, F., Bardes, A., Mialon, G., Tian, Y., et al., 2023. A cookbook of self-supervised learning. arXiv preprint URL: <https://arxiv.org/abs/2304.12210>.

- Bao, H., Dong, L., Piao, S., Wei, F., 2021. BEiT: BERT pre-training of image transformers, in: Proc. Int. Conf. Learn. Represent. (ICLR).
- Bovik, A.C., 1988. On detecting edges in speckle imagery. IEEE Trans. Acoust. Speech Signal Process. 36, 1618–1627.
- Canny, J., 1986. A computational approach to edge detection. IEEE Trans. Pattern Anal. Mach. Intell. , 679–698.
- Chen, J., Hu, M., Li, B., Elhoseiny, M., 2022a. Efficient self-supervised vision pretraining with local masked reconstruction. arXiv preprint URL: <https://arxiv.org/abs/2206.00790>.
- Chen, J., Huang, Z., Xia, R., Wu, B., Sheng, L., Sun, L., Yao, B., 2022b. Large-scale multi-class SAR image target detection dataset-1.0. <https://radars.ac.cn/web/data/getData?dataType=MSAR>.
- Chen, Y., Bruzzone, L., 2022. Self-supervised SAR-optical data fusion of Sentinel-1/2 images. IEEE Trans. Geosci. Remote Sens. 60, 1–11. doi:10.1109/GRS.2021.3128072.
- Cheng, G., Yuan, X., Yao, X., Yan, K., Zeng, Q., Xie, X., Han, J., 2023. Towards large-scale small object detection: Survey and benchmarks. IEEE Trans. Pattern Anal. Mach. Intell. 45, 13467–13488. doi:10.1109/TPAMI.2023.3290594.
- Cheng, M.M., Gao, S.H., Borji, A., Tan, Y.Q., Lin, Z., Wang, M., 2022. A highly efficient model to study the semantics of salient object detection. IEEE Trans. Pattern Anal. Mach. Intell. 44, 8006–8021. doi:10.1109/TPAMI.2021.3107956.
- Datcu, M., Huang, Z., Anghel, A., Zhao, J., Căcoveanu, R., 2023. Explainable, physics-aware, trustworthy artificial intelligence: A paradigm shift for synthetic aperture radar. IEEE Geosci. Remote Sens. Mag. 11, 8–25.
- Dellinger, F., Delon, J., Gousseau, Y., Michel, J., Tupin, F., 2014. SAR-SIFT: a SIFT-like algorithm for SAR images. IEEE Trans. Geosci. Remote Sens. 53, 453–466.
- Dong, G., Liu, H., Chanussot, J., 2020. Keypoint-based local descriptors for target recognition in SAR images: A comparative analysis. IEEE Geosci. Remote Sens. Mag. 9, 139–166.
- Dosovitskiy, A., Beyer, L., Kolesnikov, A., Weissenborn, D., Zhai, X., Unterthiner, T., Dehghani, M., Minderer, M., Heigold, G., Gelly, S., et al., 2020. An image is worth 16x16 words: Transformers for image recognition at scale. arXiv preprint URL: <https://arxiv.org/abs/2010.11929>.
- Fei-Fei, L., Krishna, R., 2022. Searching for computer vision north stars. Daedalus 151, 85–99.
- Frolind, P.O., Gustavsson, A., Lundberg, M., Ulander, L.M., 2011. Circular-aperture VHF-band synthetic aperture radar for detection of vehicles in forest concealment. IEEE Trans. Geosci. Remote Sens. 50, 1329–1339.
- Gagliardi, V., Tosti, F., Bianchini Ciampoli, L., Battagliere, M.L., D’Amato, L., Alani, A.M., Benedetto, A., 2023. Satellite remote sensing and non-destructive testing methods for transport infrastructure monitoring: Advances, challenges and perspectives. Remote Sens. 15, 418.

- Goldblum, M., Souiri, H., Ni, R., Shu, M., Prabhu, V.U., Somepalli, G., Chattopadhyay, P., Ibrahim, M., Bardes, A., Hoffman, J., Chellappa, R., Wilson, A.G., Goldstein, T., 2023. Battle of the backbones: A large-scale comparison of pretrained models across computer vision tasks, in: Proc. Adv. Neural Inf. Process. Syst. (NeurIPS). URL: <https://openreview.net/forum?id=1yOnfDpkVe>.
- He, K., Chen, X., Xie, S., Li, Y., Dollár, P., Girshick, R., 2022. Masked autoencoders are scalable vision learners, in: Proc. IEEE Comput. Soc. Conf. Comput. Vis. Pattern Recognit. (CVPR), pp. 16000–16009.
- Hou, X., Ao, W., Song, Q., Lai, J., Wang, H., Xu, F., 2020. FUSAR-Ship: Building a high-resolution SAR-AIS matchup dataset of Gaofen-3 for ship detection and recognition. Sci. China Inf. Sci. 63, 1–19.
- Huang, L., Liu, B., Li, B., Guo, W., Yu, W., Zhang, Z., Yu, W., 2017. OpenSARShip: A dataset dedicated to Sentinel-1 ship interpretation. IEEE J. Sel. Top. Appl. Earth Obs. Remote Sens. 11, 195–208.
- Huang, Z., Yao, X., Liu, Y., Dumitru, C.O., Datcu, M., Han, J., 2022. Physically explainable CNN for SAR image classification. ISPRS J. Photogramm. Remote Sens. 190, 25–37.
- Ibanez, D., Fernandez-Beltran, R., Pla, F., Yokoya, N., 2022. Masked auto-encoding spectral-spatial transformer for hyperspectral image classification. IEEE Trans. Geosci. Remote Sens. 60, 1–14.
- Kechagias-Stamatis, O., Aouf, N., 2021. Automatic target recognition on synthetic aperture radar imagery: A survey. IEEE Aerosp. Electron. Syst. Mag. 36, 56–81. doi:10.1109/MAES.2021.3049857.
- Kusk, A., Abulaitjiang, A., Dall, J., 2016. Synthetic SAR image generation using sensor, terrain and target models, in: Proc. Eur. Conf. Synth. Aperture Radar, EUSAR 2016, VDE. pp. 1–5.
- Lewis, B., Scarnati, T., Sudkamp, E., Nehrbass, J., Rosencrantz, S., Zelnio, E., 2019. A SAR dataset for ATR development: the synthetic and measured paired labeled experiment (SAMPLE), in: Proc. SPIE Conf. Algorithms SAR Imagery, pp. 39–54.
- Li, J., Yu, Z., Yu, L., Cheng, P., Chen, J., Chi, C., 2023a. A comprehensive survey on SAR ATR in deep-learning era. Remote Sens. 15, 1454.
- Li, W., Yang, W., Zhang, W., Liu, T., Liu, Y., Liu, L., 2023b. Hierarchical disentanglement-alignment network for robust SAR vehicle recognition. IEEE J. Sel. Top. Appl. Earth Obs. Remote Sens. 16, 9661–9679. doi:10.1109/JSTARS.2023.3324182.
- Li, Y., Hou, Q., Zheng, Z., Cheng, M.M., Yang, J., Li, X., 2023c. Large selective kernel network for remote sensing object detection, in: Proc. IEEE Int. Conf. Comput. Vis. (ICCV), pp. 16794–16805.
- Liu, X., Zhang, F., Hou, Z., Mian, L., Wang, Z., Zhang, J., Tang, J., 2021. Self-supervised learning: Generative or contrastive. IEEE Trans. Knowl. Data Eng. 35, 857–876.
- Liu, Y., Wu, Y.H., Wen, P., Shi, Y., Qiu, Y., Cheng, M.M., 2022. Leveraging instance-, image- and dataset-level information for weakly supervised instance segmentation. IEEE Trans. Pattern Anal. Mach. Intell. 44, 1415–1428. doi:10.1109/TPAMI.2020.3023152.
- Liu, Y., Zhang, S., Chen, J., Chen, K., Lin, D., 2023. PixMIM: Rethinking pixel reconstruction in masked image modeling. arXiv preprint URL: <https://arxiv.org/abs/2303.02416>.
- Malmgren-Hansen, D., Kusk, A., Dall, J., Nielsen, A.A., Engholm, R., Skriver, H., 2017. Improving SAR automatic target recognition models with transfer learning from simulated data. IEEE Geosci. Remote Sens. Lett. 14, 1484–1488.
- Moreira, A., Prats-Iraola, P., Younis, M., Krieger, G., Hajnsek, I., Papathanassiou, K.P., 2013. A tutorial on synthetic aperture radar. IEEE Geosci. Remote Sens. Mag. 1, 6–43. doi:10.1109/MGRS.2013.2248301.
- Pei, H., Su, M., Xu, G., Xing, M., Hong, W., 2023. Self-supervised feature representation for SAR image target classification using contrastive learning. IEEE J. Sel. Top. Appl. Earth Obs. Remote Sens. 16, 9246–9258. doi:10.1109/JSTARS.2023.3321769.
- Peng, B., Peng, B., Zhou, J., Xie, J., Liu, L., 2022. Scattering model guided adversarial examples for SAR target recognition: Attack and defense. IEEE Trans. Geosci. Remote Sens. 60, 1–17.
- Reed, C.J., Gupta, R., Li, S., Brockman, S., Funk, C., Clipp, B., Keutzer, K., Candido, S., Uyttendaele, M., Darrell, T., 2023. Scale-MAE: A scale-aware masked autoencoder for multiscale geospatial representation learning, in: Proc. IEEE Int. Conf. Comput. Vis. (ICCV), pp. 4088–4099.
- Rizzi, M., Tagliaferri, D., Tebaldini, S., Nicoli, M., Russo, I., Mazzucco, C., Monti-Guarnieri, A.V., Prati, C.M., Spagnolini, U., 2021. Navigation-aided automotive SAR imaging in urban environments, in: Proc. Int. Geosci. Remote. Sens. Symp. (IGARSS), IEEE. pp. 2979–2982.
- Ross, T.D., Bradley, J.J., Hudson, L.J., O’connor, M.P., 1999. SAR ATR: So what’s the problem? An MSTAR perspective, in: Proc. SPIE Conf. Algorithms SAR Imagery, pp. 662–672.
- Shi, B., Zhang, D., Dai, Q., Zhu, Z., Mu, Y., Wang, J., 2020. Informative dropout for robust representation learning: A shape-bias perspective, in: Int. Conf. Machin. Learn. (ICML).
- Song, S., Xu, B., Yang, J., 2016. SAR target recognition via supervised discriminative dictionary learning and sparse representation of the SAR-HOG feature. Remote Sens. 8, 683.
- Sumbul, G., De Wall, A., Kreuziger, T., Marcelino, F., Costa, H., Benevides, P., Caetano, M., Demir, B., Markl, V., 2021. BigEarthNet-MM: A large-scale, multimodal, multilabel benchmark archive for remote sensing image classification and retrieval [software and data sets]. IEEE Geosci. Remote Sens. Mag. 9, 174–180.
- Sun, G.C., Liu, Y., Xiang, J., Liu, W., Xing, M., Chen, J., 2021. Spaceborne synthetic aperture radar imaging algorithms: An overview. IEEE Geosci. Remote Sens. Mag. 10, 161–184.
- Sun, X., Lv, Y., Wang, Z., Fu, K., 2022. SCAN: Scattering characteristics analysis network for few-shot aircraft classification in high-resolution SAR images. IEEE Trans. Geosci. Remote Sens. 60, 1–17. doi:10.1109/TGRS.2022.3166174.
- Sun, X., Wang, P., Lu, W., Zhu, Z., Lu, X., He, Q., Li, J., Rong, X., Yang, Z., Chang, H., He, Q., Yang, G., Wang, R., Lu, J., Fu, K., 2023. RingMo: A remote sensing foundation model with masked image modeling. IEEE Trans. Geosci. Remote Sens. 61, 1–22. doi:10.1109/TGRS.2022.3194732.
- Tao, C., Qi, J., Zhang, G., Zhu, Q., Lu, W., Li, H., 2023. TOV: The original vision model for optical remote sensing image understanding via self-supervised learning. IEEE J. Sel. Top. Appl. Earth Obs. Remote Sens. 16, 4916–4930. doi:10.1109/JSTARS.2023.3271312.
- Touzi, R., Lopes, A., Bousquet, P., 1988. A statistical and geometrical edge detector for SAR images. IEEE Trans. Geosci. Remote Sens. 26, 764–773.
- Tsokas, A., Rysz, M., Pardalos, P.M., Dipple, K., 2022. SAR data applications in earth observation: An overview. Expert Syst. Appl. 205, 117342.
- Wang, D., Song, Y., Huang, J., An, D., Chen, L., 2022a. SAR target classification based on multiscale attention super-class network. IEEE J. Sel. Top. Appl. Earth Obs. Remote Sens. 15, 9004–9019.
- Wang, H., Song, K., Fan, J., Wang, Y., Xie, J., Zhang, Z., 2023a. Hard patches mining for masked image modeling, in: Proc. IEEE Comput. Soc. Conf. Comput. Vis. Pattern Recognit. (CVPR), pp. 10375–10385.
- Wang, H., Tang, Y., Wang, Y., Guo, J., Deng, Z.H., Han, K., 2023b. Masked image modeling with local multi-scale reconstruction, in: Proc. IEEE Comput. Soc. Conf. Comput. Vis. Pattern Recognit. (CVPR), pp. 2122–2131.
- Wang, K., Zhang, G., Leung, H., 2019. SAR target recognition based on cross-domain and cross-task transfer learning. IEEE Access 7, 153391–153399.
- Wang, Y., Albrecht, C.M., Braham, N.A.A., Mou, L., Zhu, X.X., 2022b. Self-supervised learning in remote sensing: A review. IEEE Geosci. Remote Sens. Mag. 10, 213–247. doi:10.1109/MGRS.2022.3198244.
- Wang, Y., Hernández, H.H., Albrecht, C.M., Zhu, X.X., 2023c. Feature guided masked autoencoder for self-supervised learning in remote sensing. arXiv preprint URL: <https://arxiv.org/abs/2310.18653>.
- Wei, C., Fan, H., Xie, S., Wu, C.Y., Yuille, A., Feichtenhofer, C., 2022. Masked feature prediction for self-supervised visual pre-training, in: Proc. IEEE Comput. Soc. Conf. Comput. Vis. Pattern Recognit. (CVPR), pp. 14668–14678.
- Wen, Z., Liu, Z., Zhang, S., Pan, Q., 2021. Rotation awareness based self-supervised learning for SAR target recognition with limited training samples. IEEE Trans. Image Process. 30, 7266–7279.

- Wu, K., Peng, H., Chen, M., Fu, J., Chao, H., 2021. Rethinking and improving relative position encoding for vision transformer, in: Proc. IEEE Comput. Soc. Conf. Comput. Vis. Pattern Recognit. (CVPR), pp. 10033–10041.
- Xia, R., Chen, J., Huang, Z., Wan, H., Wu, B., Sun, L., Yao, B., Xiang, H., Xing, M., 2022. CRTransSAR: A visual transformer based on contextual joint representation learning for SAR ship detection. *Remote Sens.* 14, 1488.
- Xie, J., Li, W., Zhan, X., Liu, Z., Ong, Y.S., Loy, C.C., 2023a. Masked frequency modeling for self-supervised visual pre-training, in: Proc. Int. Conf. Learn. Represent. (ICLR).
- Xie, Z., Geng, Z., Hu, J., Zhang, Z., Hu, H., Cao, Y., 2023b. Revealing the dark secrets of masked image modeling, in: Proc. IEEE Comput. Soc. Conf. Comput. Vis. Pattern Recognit. (CVPR), pp. 14475–14485.
- Xie, Z., Zhang, Z., Cao, Y., Lin, Y., Bao, J., Yao, Z., Dai, Q., Hu, H., 2022. SimMIM: A simple framework for masked image modeling, in: Proc. IEEE Comput. Soc. Conf. Comput. Vis. Pattern Recognit. (CVPR), pp. 9653–9663.
- Xie, Z., Zhang, Z., Cao, Y., Lin, Y., Wei, Y., Dai, Q., Hu, H., 2023c. On data scaling in masked image modeling, in: Proc. IEEE Comput. Soc. Conf. Comput. Vis. Pattern Recognit. (CVPR), pp. 10365–10374.
- Zhai, Y., Zhou, W., Sun, B., Li, J., Ke, Q., Ying, Z., Gan, J., Mai, C., Labati, R.D., Piuri, V., Scotti, F., 2022. Weakly contrastive learning via batch instance discrimination and feature clustering for small sample SAR ATR. *IEEE Trans. Geosci. Remote Sens.* 60, 1–17. doi:10.1109/TGRS.2021.3066195.
- Zhao, Y., Zhao, L., Liu, Z., Hu, D., Kuang, G., Liu, L., 2022. Attentional feature refinement and alignment network for aircraft detection in SAR imagery. *IEEE Trans. Geosci. Remote Sens.* 60, 1–16. doi:10.1109/TGRS.2021.3139994.
- Zhou, K., Liu, Z., Qiao, Y., Xiang, T., Loy, C.C., 2023a. Domain generalization: A survey. *IEEE Trans. Pattern Anal. Mach. Intell.* 45, 4396–4415.
- Zhou, Y., Chia, M.A., Wagner, S.K., Ayhan, M.S., Williamson, D.J., Struyven, R.R., Liu, T., Xu, M., Lozano, M.G., Woodward-Court, P., et al., 2023b. A foundation model for generalizable disease detection from retinal images. *Nature*, 1–8.